

© Copyright 2023 American Meteorological Society (AMS). For permission to reuse any portion of this Work, please contact permissions@ametsoc.org. Any use of material in this Work that is determined to be “fair use” under Section 107 of the U.S. Copyright Act (17 U.S. Code § 107) or that satisfies the conditions specified in Section 108 of the U.S. Copyright Act (17 USC § 108) does not require the AMS’s permission. Republication, systematic reproduction, posting in electronic form, such as on a website or in a searchable database, or other uses of this material, except as exempted by the above statement, requires written permission or a license from the AMS. All AMS journals and monograph publications are registered with the Copyright Clearance Center (<https://www.copyright.com>). Additional details are provided in the AMS Copyright Policy statement, available on the AMS website (<https://www.ametsoc.org/PUBSCopyrightPolicy>).

Diagnosing Product Variability in the Soil Moisture Response to Precipitation on the Tibetan Plateau

X. MENG^a, M. DENG,^{a,b} J. TALIB,^c C. M. TAYLOR,^{c,d} P. WU,^e S. LYU,^f H. CHEN,^a Z. LI,^a AND L. ZHAO^a

^a Key Laboratory of Land Surface Process and Climate Change in Cold and Arid Regions, Northwest Institute of Eco-Environment and Resources, Chinese Academy of Sciences, Lanzhou, China

^b University of Chinese Academy of Sciences, Beijing, China

^c U.K. Centre for Ecology and Hydrology, Wallingford, United Kingdom

^d National Centre for Earth Observation, Wallingford, United Kingdom

^e Met Office Hadley Centre, Exeter, United Kingdom

^f College of Atmospheric Sciences, Chengdu University of Information Technology, Chengdu, China

(Manuscript received 6 October 2022, in final form 19 December 2022)

ABSTRACT: Previous studies show that some soil moisture products have a good agreement with in situ measurements on the Tibetan Plateau (TP). However, the soil moisture response to precipitation variability in different products is yet to be assessed. In this study, we focus on the soil moisture response to precipitation variability across weekly to decadal time scales in satellite observations and reanalyses. The response of soil moisture to precipitation variability differs between products, with large uncertainties observed for variations in weekly accumulated precipitation. Using June 2009 as an example, weekly mean anomalous soil moisture varies by up to 25% between products. Across decadal time scales, soil moisture trends vary spatially and across different products. In light of the soil moisture response to precipitation at different time scales, we conclude that remote sensing products developed as part of the European Space Agency's (ESA) Water Cycle Multimission Observation Strategy and Soil Moisture Climate Change Initiative (CCI) projects are the most reliable, followed by the Global Land Evaporation Amsterdam Model (GLEAM) dataset. Even products that strongly agree with in situ observations on daily time scales, such as the Global Land Data Assimilation System (GLDAS), show inconsistent soil moisture responses to decadal precipitation trends. European Centre for Medium-Range Weather Forecasts (ECWMF) reanalysis products have a relatively poor agreement with in situ observations compared to satellite observations and land-only reanalysis datasets. Unsurprisingly, products which show a consistent soil moisture response to precipitation variability are those mostly aligned to observations or describe the physical relationship between soil moisture and precipitation well.

SIGNIFICANCE STATEMENT: We focus on soil moisture responses to precipitation across weekly to decadal time scales by using multiple satellite observations and reanalysis products. Several soil moisture products illustrate good consistency with in situ measurements in different biomes on the Tibetan Plateau, while the response to precipitation variability differs between products, with large uncertainties observed for variations in weekly accumulated precipitation. The response of soil moisture to decadal trends in boreal summer precipitation varies spatially and temporally across products. Based on the assessments of the soil moisture response to precipitation variability across different time scales, we conclude that remote sensing products developed as part of the European Space Agency's Water Cycle Multimission Observation Strategy and Soil Moisture Climate Change Initiative (CCI) projects are the most reliable, followed by the Global Land Evaporation Amsterdam Model (GLEAM) dataset. Reanalysis products from ECWMF show inconsistent soil moisture responses to precipitation. The results highlight the importance of using multiple soil moisture products to understand the surface response to precipitation variability and to inform developments in soil moisture modeling and satellite retrievals.

KEYWORDS: Soil moisture; Hydrometeorology; Satellite observations; Trends; Precipitation

1. Introduction

Subseasonal to decadal atmospheric prediction relies on climate system components with substantial “memory” including the land surface, ocean, and sea ice (Koster and Suarez 2001). Soil moisture is a key memory variable as it regulates surface processes, which influence the surface water and energy balance and biogeochemical cycles. Land–atmosphere feedbacks associated with soil moisture can substantially

impact precipitation and radiation anomalies while influencing local, regional, and global climate (Seneviratne et al. 2010).

Soil moisture varies evidently in both time and space, because it is controlled by multiple elements, for example, precipitation, vegetation characteristics, topographic distribution, and soil properties. Soil moisture dynamics is the main process controlling meteorological processes, soil biogeochemistry, plant growth and nutrient cycles (Daly and Porporato 2005). Precipitation variability is among other important factors affecting the spatial and temporal pattern in soil moisture. In semiarid biomes, it was found that only large precipitation

Corresponding author: X. Meng, mxh@lzb.ac.cn

DOI: 10.1175/JHM-D-22-0181.1

© 2023 American Meteorological Society. For information regarding reuse of this content and general copyright information, consult the AMS Copyright Policy (www.ametsoc.org/PUBSReuseLicenses).

Brought to you by UK CENTRE FOR ECOLOGY & HYDROLOGY | Unauthenticated | Downloaded 04/13/23 08:03 AM UTC

events (15 and 20 mm) enhanced soil moisture and facilitated the penetration of water into the deeper soil layers at the grassland surface lying in northeastern Colorado in the United States (Heisler-White et al. 2008). Although soil moisture anomalies occurrences depend on large precipitation events, it was found frequent rainfall usually results in soil moisture responses other than individual rainfall events (Sun et al. 2015).

The Tibetan Plateau (TP), located in southwest China, is the largest and highest elevated plateau in the world with an average height above 4000 m. It extends approximately 1000 km meridionally and 2500 km zonally. With its vast distribution of glaciers, permafrost and snow, the TP is a vital water source for many large rivers across Asia including the Yangtze, Yellow, Indus, and Mekong (Yao et al. 2019). In addition to its “Asia Water Tower” role (Yao et al. 2012; You et al. 2016; Immerzeel et al. 2020; Yao et al. 2022), it has also been shown to affect local, regional, and global atmospheric conditions due to its strong thermal and dynamic influence on the atmosphere (Ma et al. 2009; Duan et al. 2012; Wu et al. 2012; Wan et al. 2017; Barton et al. 2021; Talib et al. 2021; Ma and Zhang 2022; Yan et al. 2022).

In situ observations are capable of providing accurate soil moisture measurements. Based on these observations, the response of soil moisture to precipitation intensity and frequency has been examined across different biomes and regions on the TP (Zhu et al. 2017; Dai et al. 2019, 2022). For example, temporal changes in soil moisture at depths of 0–20 and 40–60 cm are consistent with precipitation variations across alpine meadow and shrub biomes in the northeast TP (Dai et al. 2022). For larger soil moisture depths, seasonal variations in infiltration are independent to the precipitation intensity (Dai et al. 2019). Over the Tanggula permafrost region across the central TP for example, extreme precipitation has a large influence on infiltration characteristics (Zhu et al. 2017). The intensity of an extreme precipitation event can influence the persistence of anomalous soil moisture conditions.

However, in situ measurements across the TP are spatially limited, which is problematic given the substantial spatial variability in soil moisture (Zhang et al. 2018). Satellite products and reanalyses provide a better mapping of soil moisture across regional scales. Microwave remote sensing measurements afford the possibility to obtain frequent, global sampling of soil moisture over a large fraction of Earth’s land surface (Njoku and Entekhabi 1996). Reanalyses, on the other hand, are considered an essential substitute where satellite observations are not available (Al-Yaari et al. 2014; Baatz et al. 2021). However, before using these different soil moisture products, it is necessary to evaluate them across different spatial and temporal scales.

In spite of the hostile environment on the TP and logistical challenges associated with developing in situ observational networks, several site observations and three soil moisture networks have recently been set up across different biomes (Su et al. 2011; Yang et al. 2013). Several studies have evaluated soil moisture products across the TP using these in situ observations (Chen et al. 2013; Su et al. 2013; Al-Yaari et al. 2014; Zeng et al. 2015; Zhang et al. 2018). For example, Zeng et al. (2015), and Zhang et al. (2018), compared different soil

moisture products to in situ measurements. They concluded that instantaneous soil moisture observations were well represented by satellite and reanalysis products, especially for the remote sensing products developed as part of the European Space Agency’s (ESA) Water Cycle Multimission Observation Strategy and Soil Moisture Climate Change Initiative projects (hereafter referred to as CCI; Liu et al. 2012; Wagner et al. 2012), the Advanced Scatterometer (ASCAT) retrieval products from the European Meteorological Satellite (EUMETSAT; Wagner et al. 2010), and the assimilation products developed by Global Land Data Assimilation System (GLDAS; Rodell et al. 2004). Products also successfully capture the soil moisture response to daily precipitation events (Zhang et al. 2018).

While previous studies have focused on the agreement between in situ measurements and absolute soil moisture values across the TP (Zhang et al. 2018), and the instantaneous response of soil moisture to individual precipitation events at site-based scale, in this study we investigate the agreement between products in the soil moisture response to precipitation variability on weekly and decadal time scales at the shallow layer and discuss the consistency of soil moisture dynamics in these two time scales among the products on the TP. Section 2 introduces the different products and statistical techniques utilized in this study. Section 3 investigates products variability in soil moisture response to precipitation, across weekly and decadal time scales. Section 3a describes the spatial distribution of soil moisture on the TP. Section 3b analyses the soil moisture response to weekly precipitation fluctuations during boreal summer. Meanwhile, sections 3c and 3d analyze the soil moisture response to interannual and decadal climate variability, with section 3d focusing on the soil moisture response across different biomes. Sections 4 and 5 finish the paper with discussion and conclusions, respectively.

2. Data and methods

a. Remote sensing products

This study utilizes the great efforts of researchers working on the development of microwave-based soil moisture retrieval algorithms by analyzing several soil moisture products, including the Advanced Microwave Scanning Radiometer for Earth Observing System (AMSR-E) on the National Aeronautics and Space Administration (NASA) *Aqua* satellite and the Advanced Microwave Scanning Radiometer 2 (AMSR2) products generated by the Land Parameter Retrieval Model (LPRM; Owe et al. 2008) and the ESA’s CCI (Liu et al. 2012; Wagner et al. 2012). Table 1 provides details of each individual remote sensing soil moisture product.

The AMSR-E/AMSR2 products were the first attempt to produce soil moisture readings at an accuracy higher than $0.06 \text{ m}^3 \text{ m}^{-3}$ (Njoku et al. 2003; Njoku and Chan 2006). Different products were released using alternative algorithms, including the NASA soil moisture product (version 6, i.e., the AMSRE/2 NASA product; Njoku and Chan 2006), the Japan Aerospace Exploration Agency (JAXA) soil moisture product (version 7, i.e., the AMSRE/2 JAXA product; Koike et al. 2004), and the Land Parameter Retrieval Model (LPRM) soil

TABLE 1. Information of remote sensing soil moisture products used in this work.

Data name	Time period	Temporal resolution	Spatial resolution	Layer	Passing time
AMSR-E/2 LPRM	2002–16	Daily	$0.25^\circ \times 0.25^\circ$	0–5 cm	0130/1330 LT
CCI	1980–2016	Daily	$0.25^\circ \times 0.25^\circ$	0–5 cm	Multiple overpass times depending on sensor

moisture product (version 2, i.e., the AMSRE/2 LPRM product; Owe et al. 2008). In this paper, we use the LPRM soil moisture product as it performs best during daytime hours in the unfrozen season on the TP (Zeng et al. 2015). The LPRM soil moisture product is generated using a three-parameter method, computing the vegetation optical depth as a function of the soil dielectric constant and the microwave polarization difference index (MPDI; Owe et al. 2001; Meesters et al. 2005), retrieving land surface temperature from the vertically polarized Ka-band observations using an empirical regression model (Holmes et al. 2009), and calculating soil moisture in the radiative transfer equation through a nonlinear interactive procedure (Njoku et al. 2005).

The ESA CCI soil moisture product merges several data sources, including the Special Sensor Microwave Imager (SSM/I), the Scanning Multichannel Microwave Radiometer (SSM/R), the Tropical Rainfall Measuring Mission (TRMM) Microwave Imager, the AMSR-E product, the ASCAT active datasets, the WindSat microwave imaging radiometer, AMSR2 passive datasets, and the scatterometers (SCAT; Liu et al. 2012; Wagner et al. 2012). These soil moisture products have already been used to understand surface processes on the TP (Meng et al. 2018; Deng et al. 2020).

b. Reanalysis products

In this study, several widely used reanalysis products are analyzed including: the European Centre for Medium-Range Weather Forecasts (ECWMF) reanalyses (Dee et al. 2011) versions interim (ERA-I) and 5.0 (ERA5); the Modern-Era Retrospective Analysis for Research and Applications (MERRA) land-only product, produced by the Global Modeling and Assimilation Office of NASA (Rienecker et al. 2011); the Global Land Data Assimilation System (GLDAS; Rodell et al. 2004); and the Global Land Evaporation Amsterdam Model (GLEAM) dataset, developed by Vrije University Amsterdam and ESA (Miralles et al. 2011; Martens et al. 2017). Details of the products are in Table 2.

ERA-I and ERA5 are two global atmosphere reanalysis datasets generated by different versions of ECMWF models (Dee et al. 2011; Hersbach et al. 2020). As a superseded version of ERA-I, ERA5 provides hourly estimates for more

variables of the atmosphere, land, and ocean than ERA-I, with a higher spatial resolution of 30 km. In addition, ERA5 incorporates more historical observations using sophisticated modeling and data assimilation systems, particularly for the estimation of precipitation, evaporation, and soil moisture (Hersbach et al. 2020). Unlike ERA-I, ERA5 assimilates soil moisture from scatterometer data. In this paper, we use the surface layer of 7 cm depth from both ECMWF reanalyses.

GLDAS is developed to generate optimal fields of land surface states and fluxes by integrating satellite- and ground-based observational data products, using land surface modeling and data assimilation techniques (Rodell et al. 2004). Two datasets from the Noah LSM model were used in the current study because of different time durations; version 2.0 runs from 1948 to 2010 while version 2.1 begins in 2000 and continues to the present day (Rodell et al. 2004). For GLDAS-2.0, the model was forced entirely with the Princeton meteorological forcing data (Sheffield et al. 2006). For GLDAS-2.1, it was started on 1 January 2000 using the conditions from the GLDAS-2.0 simulation, forced with National Oceanic and Atmospheric Administration's Global Data Assimilation System atmospheric analysis fields (Derber et al. 1991), the disaggregated Global Precipitation Climatology Project (GPCP) precipitation fields (Adler et al. 2003), and the Air Force Weather Agency's Agricultural Meteorological modeling system radiation fields, which became available for 1 March 2001 onward.

The MERRA land-only analysis product used in this study was generated using more realistic precipitation forcing than provided by the atmospheric reanalysis. The spatial resolution is 0.625° longitude \times 0.5° latitude and we use the top layer representing 2 cm (Rienecker et al. 2011).

In GLEAM, land surface evaporation is divided into different components including transpiration, bare-soil evaporation, interception loss, open-water evaporation, and sublimation (Miralles et al. 2011; Martens et al. 2017). The forcing data are based on reanalysis net radiation and air temperature, and satellite and gauged-based precipitation. GLEAM assimilates the satellite-observed soil moisture. In this study, we used the v3a datasets.

TABLE 2. Information of reanalysis soil moisture products used in this work.

Data name	Time period	Temporal resolution	Spatial resolution	Layer	Analysis time
ERA-I	1980–2016	3-hourly	$0.25^\circ \times 0.25^\circ$	0–7 cm	0000 UTC
ERA5	1980–2016	3-hourly	$0.25^\circ \times 0.25^\circ$	0–7 cm	0000 UTC
GLDAS-Noah-2.1	1980–2016	3-hourly	$0.25^\circ \times 0.25^\circ$	0–10 cm	0000 UTC
MERRA	1980–2016	3-hourly	$0.625^\circ \times 0.5^\circ$	0–2 cm	0000 UTC
GLEAM	1980–2016	Daily	$0.25^\circ \times 0.25^\circ$	0–10 cm	0000 UTC

TABLE 3. Information of observed precipitation and air temperature products used in this study.

Data	Time period	Temporal resolution	Spatial resolution
Precipitation	1980–2016	Monthly	$0.5^\circ \times 0.5^\circ$
Temperature	1980–2016	Monthly	$0.5^\circ \times 0.5^\circ$
CMORPH precipitation	2008–16	Hourly	$0.1^\circ \times 0.1^\circ$

c. The meteorological observations

Observations of air temperature and precipitation from 1961 to 2016 are obtained from the National Meteorological Information Center (NMIC), China Meteorological Administration (CMA). These data had already been quality controlled and interpolated to 0.5° latitude \times 0.5° longitude grid (Zhao et al. 2014). However, due to the arduous environment across the western side of the TP, most of the stations are located in the east. In addition, we used an hourly precipitation product on a 0.1° latitude \times 0.1° longitude grid generated by merging the Automatic Weather Station (AWS) observations using the Climate Prediction Center morphing technique (CMORPH). The CMORPH precipitation data were derived from NMIC too. Table 3 provides a summary of meteorological observations used in this study. For precipitation data, in the weekly responses, we used the CMORPH $0.1^\circ \times 0.1^\circ$ hourly precipitation data, while in the decadal time scales, we used $0.5^\circ \times 0.5^\circ$ monthly precipitation data.

d. Methods

All datasets were resampled to $0.25^\circ \times 0.25^\circ$ by inverse distance weight interpolation to be spatially consistent among datasets in the spatial scales. Correlation analysis including temporal and spatial correlation was used to assess soil moisture response to precipitation changes across weekly to decadal time scales.

A second-order partial correlation was used to examine the decadal response of soil moisture to precipitation, surface air temperature, and leaf area index (LAI). In the second-order partial correlation, we consider four variables in a time series as x_i, x_j, x_h, x_m , with correlation coefficients between the four variables of $r_{ij}, r_{ih}, r_{im}, \dots$, etc. Then the partial correlation between x_i and x_j excluding the influence of the two other variables x_h and x_m can be calculated as

$$r_{ij, hm} = \frac{r_{ij,h} - r_{im,h}r_{jm,h}}{\sqrt{(1 - r_{im,h}^2)(1 - r_{jm,h}^2)}}, \quad (1)$$

where

$$r_{ij,h} = \frac{r_{ij} - r_{ih}r_{jh}}{\sqrt{(1 - r_{ih}^2)(1 - r_{jh}^2)}}. \quad (2)$$

3. Results

a. Spatial distribution of soil moisture on the TP

To understand the soil moisture response to precipitation variability on the TP, we first investigate the climatology in each product. Figure 1 shows the boreal summer (June–August)

climatology of absolute soil moisture in each of the products, alongside the climatological precipitation and near-surface air temperature. As several remote sensing products have time periods with no data, we only show the climatology at grid points with daily values for two thirds of the time series. In addition, Fig. 1 highlights three climate zones across the TP, arid, semiarid, and semihumid, which are defined using the aridity index (AI) from the United Nations Environmental Program (UNEP; Oliver 1980). Boreal summer precipitation across the TP increases from the northwest to the southeast, with precipitation primarily controlling the three climatic zones. The highest temperatures are observed in regions on the northwestern and southern edges of the TP as well as the driest area in the north, and southern edge of TP show higher temperature than other regions, while the west of the TP has the lowest temperature due to high elevation.

Across all products a similar soil moisture gradient is observed with moisture increasing from the northwest to the southeast. However, climatological soil moisture values vary between products. The soil moisture gradient between the northwest and the southeast is greatest in AMSR (AMSR-E/AMSR2), followed by ERA5. The strength of the soil moisture gradient partly controls whether soil moisture differences are observed in different climatic zones. In the remote sensing products, AMSR illustrates stronger soil moisture differences between semiarid and semihumid regions. CCI, on the other hand, shows similar moisture values across both semiarid and semihumid regions. CCI is the merged product using multiple microwave soil moisture products, while AMSR is the product with the largest soil moisture gradient. Zeng et al. (2015) show that AMSR has a poor agreement with observations with daily soil moisture values having a correlation coefficient of 0.24 with in situ observations. With regards to reanalysis products, GLDAS, MERRA, and ERA-I show similar moisture gradients and values across the TP. GLEAM and ERA5 show the largest moisture gradients with ERA5 showing wet conditions across the typically semiarid region. There are several possible reasons for soil moisture differences among reanalysis products including different precipitation forcings, different model formulations including soil and vegetation properties, and different surface layer depths.

b. Soil moisture response to weekly precipitation variability

To understand differences between products in the soil moisture response to weekly precipitation variations, we first illustrate how weekly rainfall variability affects soil moisture anomalies. Using June 2009 as an example boreal summer season, Figs. 2–4 show the weekly accumulated precipitation and soil moisture anomaly at the last day of each week in satellite (Fig. 2) and reanalysis (Figs. 3 and 4) products. Values in each panel indicate spatial correlation coefficients between the weekly accumulated precipitation and soil moisture anomalies, showing consistency exists between them. During the beginning of June, thawing increases soil moisture across the TP (Chen et al. 2013). However, when considering soil

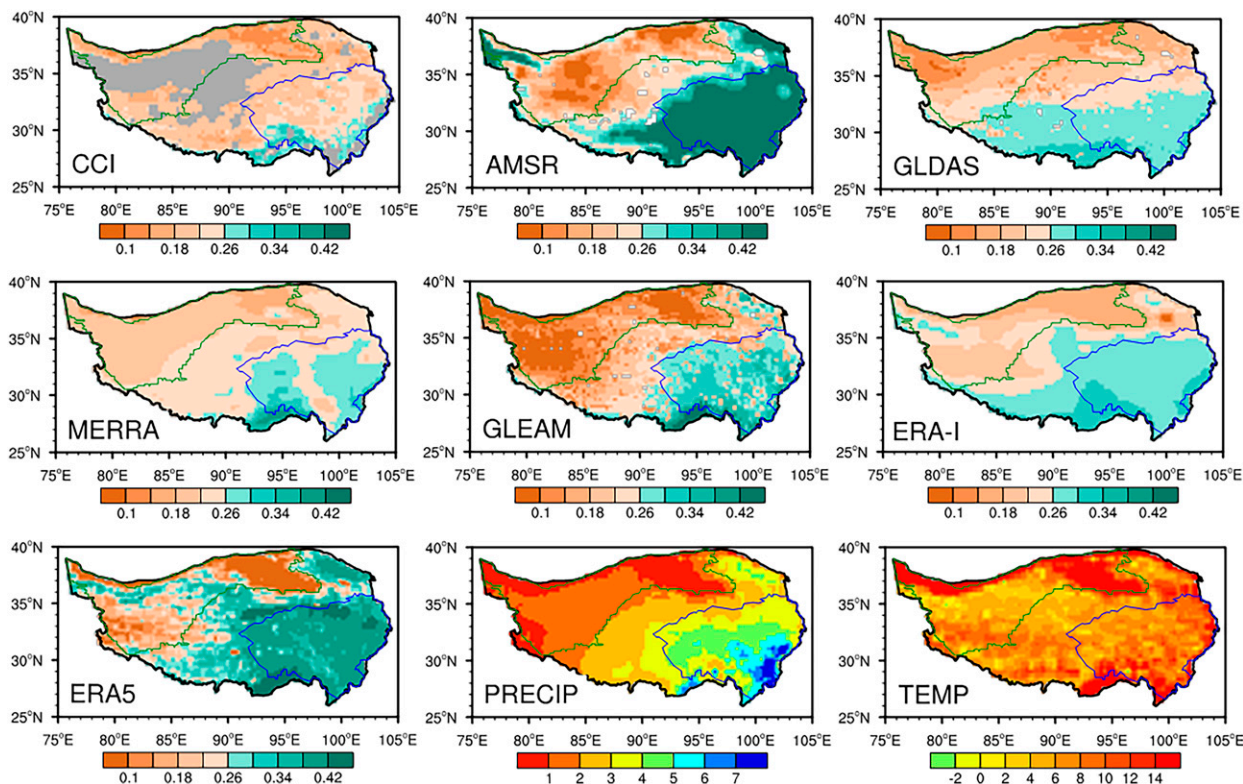


FIG. 1. Climatological soil moisture ($\text{m}^3 \text{m}^{-3}$) in boreal summer for different satellite and reanalysis products. We also show climatological CMA precipitation (mm day^{-1}) and air temperature ($^{\circ}\text{C}$). All panels show climatology values for 1980–2016, apart from AMSR soil moisture, which is for 2003–10. Gray shading indicates regions with one-third of the data missing. The green line separates arid and semiarid regions, while the blue line separates semiarid and semihumid climate zones.

moisture anomalies, spatial and temporal variations are predominantly driven by precipitation. For example, in the third and fourth weeks of June, heavy rainfall occurs in the south-east of the TP, and remote sensing products show this is

accompanied by increased soil moisture (Fig. 2). Spatial correlation coefficients between precipitation and soil moisture anomalies increase after the second week of June, consistent with rainfall driving soil moisture variability.

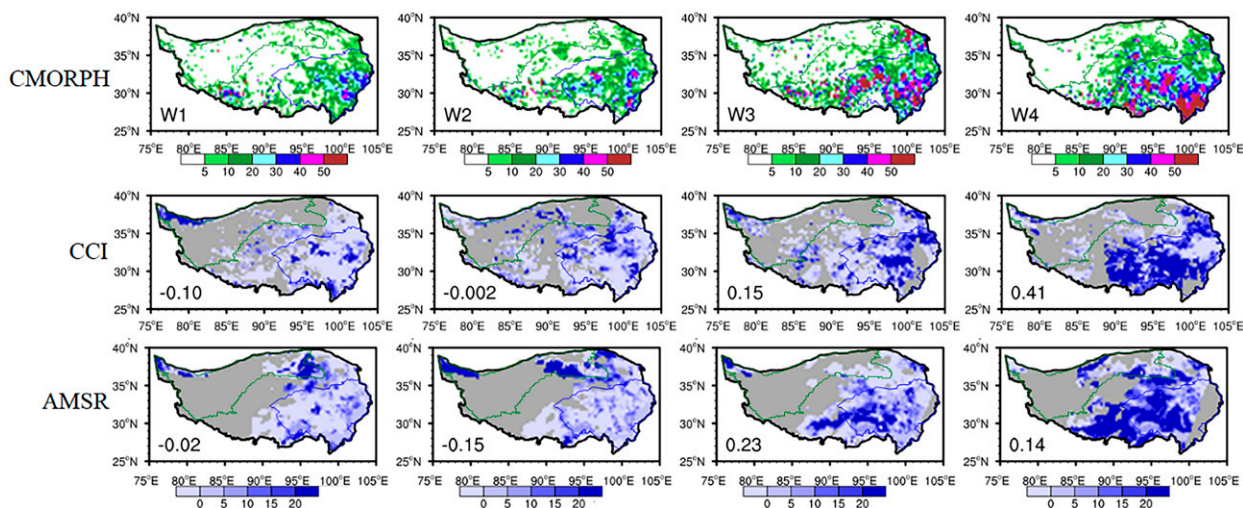


FIG. 2. Distribution of weekly accumulated CMORPH precipitation (mm week^{-1}) and soil moisture anomalies (%) in CCI and AMSR at the last day of each week during June 2009. Values in each panel indicate spatial correlation coefficients between the weekly accumulated precipitation and soil moisture anomalies. Gray shading indicates missing values.

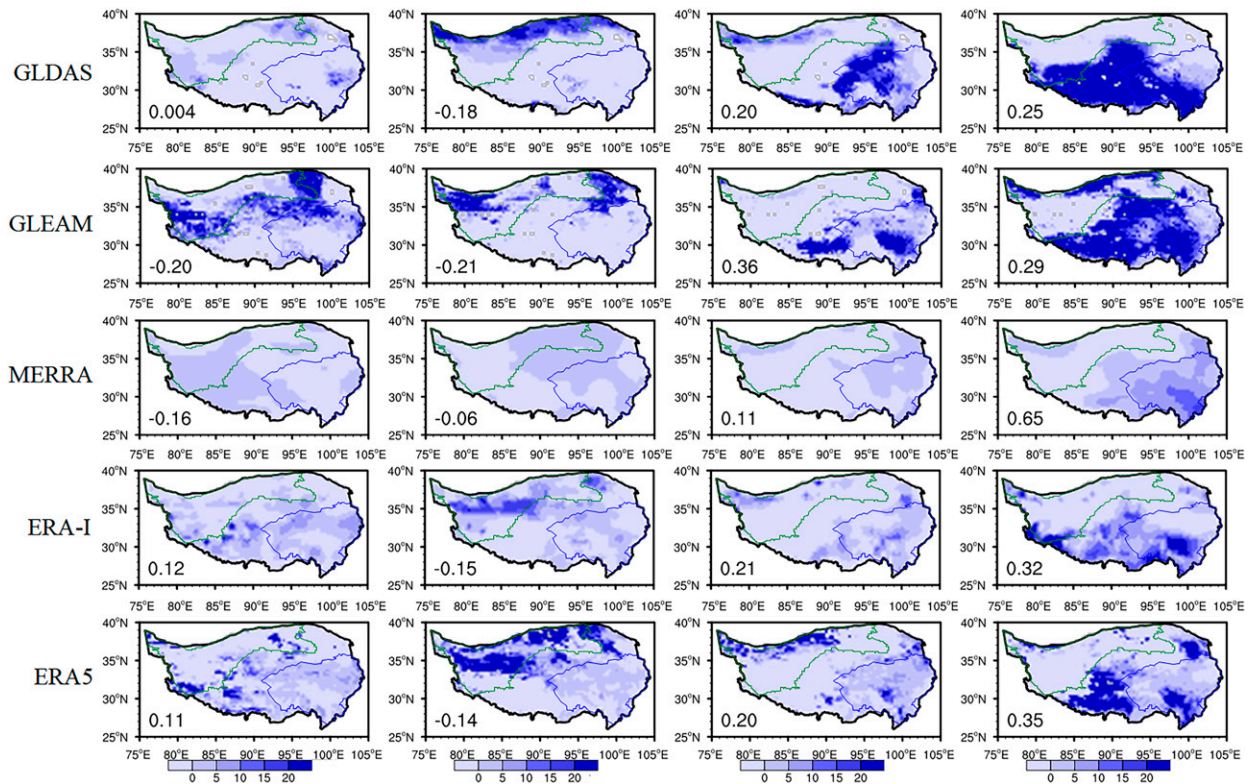


FIG. 3. Soil moisture anomalies (%; only positive anomalies are shown) in GLDAS, GLEAM, MERRA, ERA-I, and ERA5 at the last day of each week during June 2009. Values in each panel indicate spatial correlation coefficients between the weekly accumulated precipitation in Fig. 2 and soil moisture anomalies.

As for reanalyses, the sensitivity of soil moisture to weekly accumulated precipitation during June 2009 varies substantially between products, especially across central and eastern parts of the TP (Fig. 3). Considering the last two weeks of June 2009, when the imprint of rainfall on satellite soil moisture estimates is clear (Fig. 2), positive soil moisture anomalies develop in central and eastern TP in GLDAS, ERA5, GLEAM, and to a lesser extent, ERA-I (Fig. 3). We also calculate the spatial correlation coefficient between the weekly accumulated precipitation for each product and its associated anomalous soil moisture at the end of the week. As to the spatial consistency between anomalous soil moisture and CMORPH precipitation, smaller spatial correlation coefficients are observed during the last week of June 2009 in all reanalysis products, except for MERRA, compared to CCI. Smaller correlation coefficients in Fig. 3 are most likely related to differing qualities of reanalysis precipitation datasets. Figure 4 shows the spatial distribution of weekly accumulated precipitation in reanalysis products, except for GLEAM which is not available. In GLDAS, precipitation forcing is provided by GPCP (Adler et al. 2003), while in ERA-I and ERA5, precipitation is simulated by an atmospheric model which is unlikely to capture realistic small-scale precipitation features. For ERA5, precipitation biases are reduced to some extent by the assimilation of ASCAT soil moisture observations (Hersbach et al. 2020). Spatial correlation coefficients

are larger when using reanalysis precipitation predictions instead of CMORPH, except for ERA5 in the last week. This illustrates a better agreement between precipitation and soil moisture when using weekly accumulated precipitation from the corresponding reanalysis product instead of merged observational precipitation.

Through analyzing soil moisture anomalies during June 2009 it is evident that inconsistencies exist between satellite and reanalysis products (Figs. 2–4). We now generalize these findings by considering pixel-wise temporal correlations between soil moisture anomalies and antecedent precipitation accumulations based on CMORPH for boreal summer months (JJA) in 2008 and 2016. We compare soil moisture anomalies on day d relative to a 30-day rolling mean including 15 days before and after day d , with accumulated precipitation between days $d - N$ and d . We vary N between 1 and 10 and for each pixel identify the optimal value of N that produces the largest correlation coefficient (N_{opt}). Figure 5 shows that for most products across the majority of the TP, N_{opt} is typically between 5 and 10 days. There is some consistency among all products except for MERRA which has longer time scales in more humid regions, and shorter time scales in semiarid and arid regions. For MERRA, we hypothesize that low values of N_{opt} are due to a shallow depth (2 cm, Table 2) and therefore the shortest soil moisture memory.

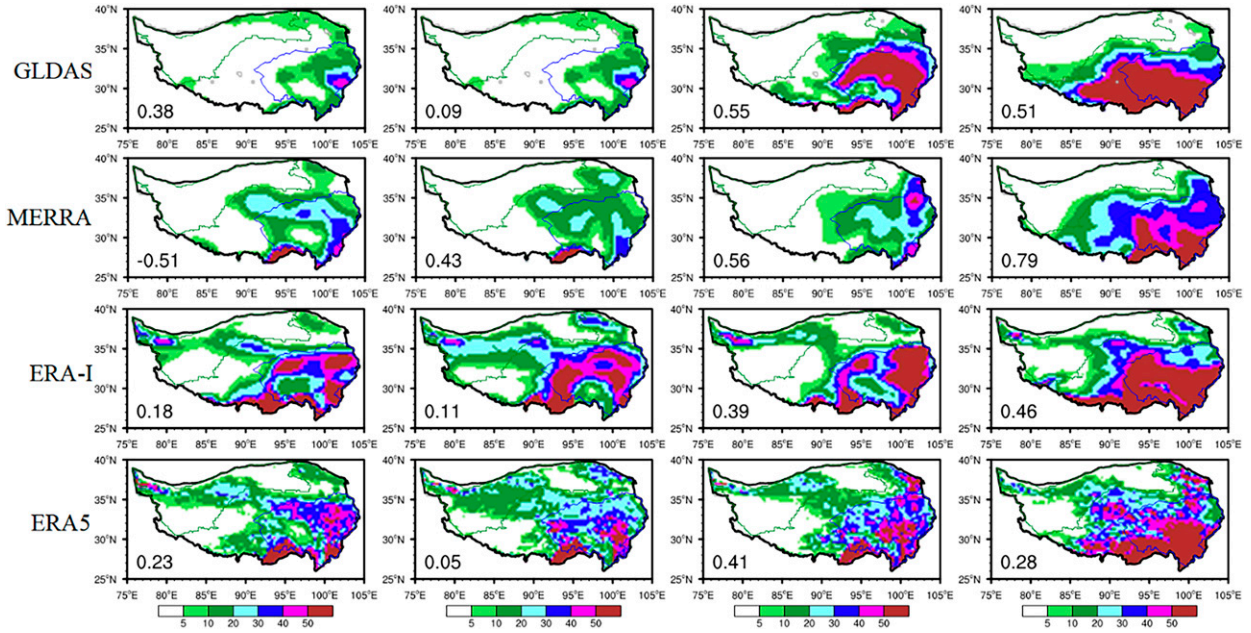


FIG. 4. Distribution of weekly accumulated precipitation (mm week^{-1}) in GLDAS, MERRA, ERA-I, and ERA5 in June 2009. Values in each panel indicate spatial correlation coefficients between the weekly accumulated precipitation in Fig. 2 and precipitation from each product.

Maps of correlation coefficients at N_{opt} indicate a ranking among products in their sensitivity to CMORPH precipitation (Fig. 6). There is a marked northwest to southeast gradient in correlation values which is shared across all the products.

There are multiple factors which may be responsible for this spatial gradient including, a higher number of in situ observations across the southeast compared to the northwest, or a minimal number of precipitating days which influence surface

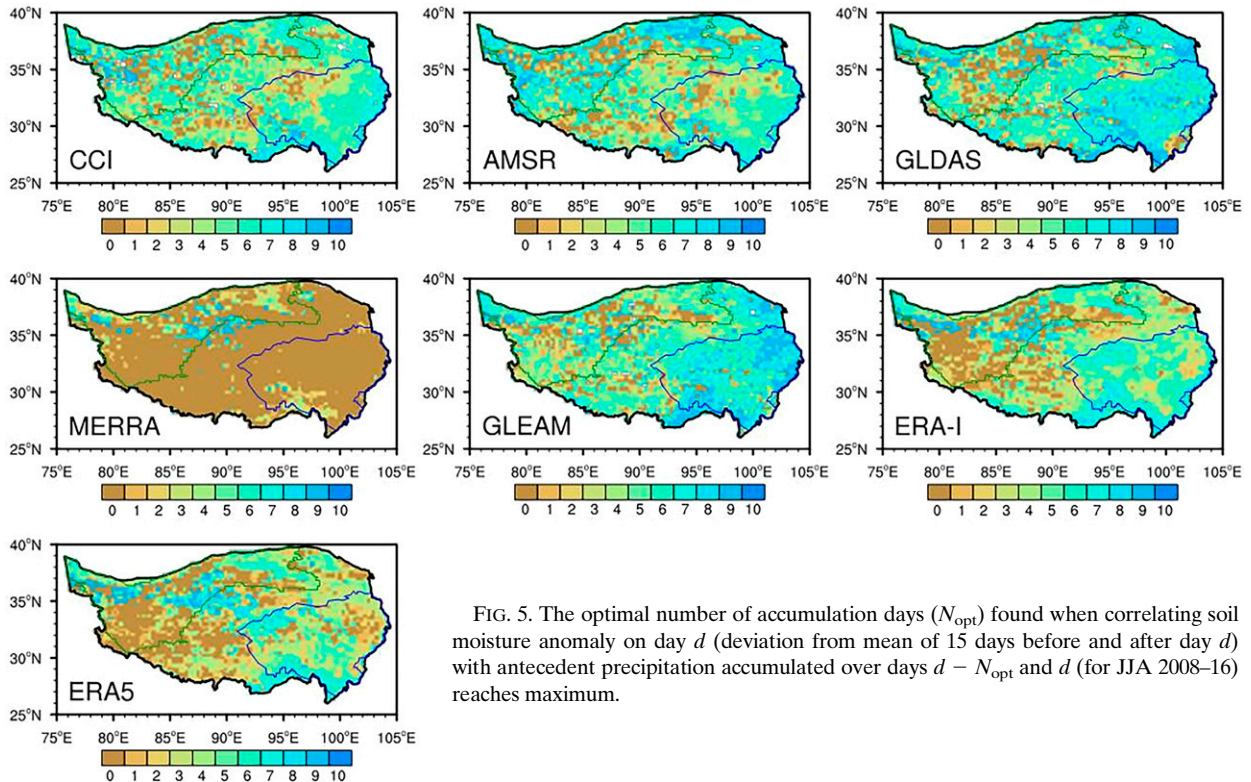


FIG. 5. The optimal number of accumulation days (N_{opt}) found when correlating soil moisture anomaly on day d (deviation from mean of 15 days before and after day d) with antecedent precipitation accumulated over days $d - N_{\text{opt}}$ and d (for JJA 2008–16) reaches maximum.

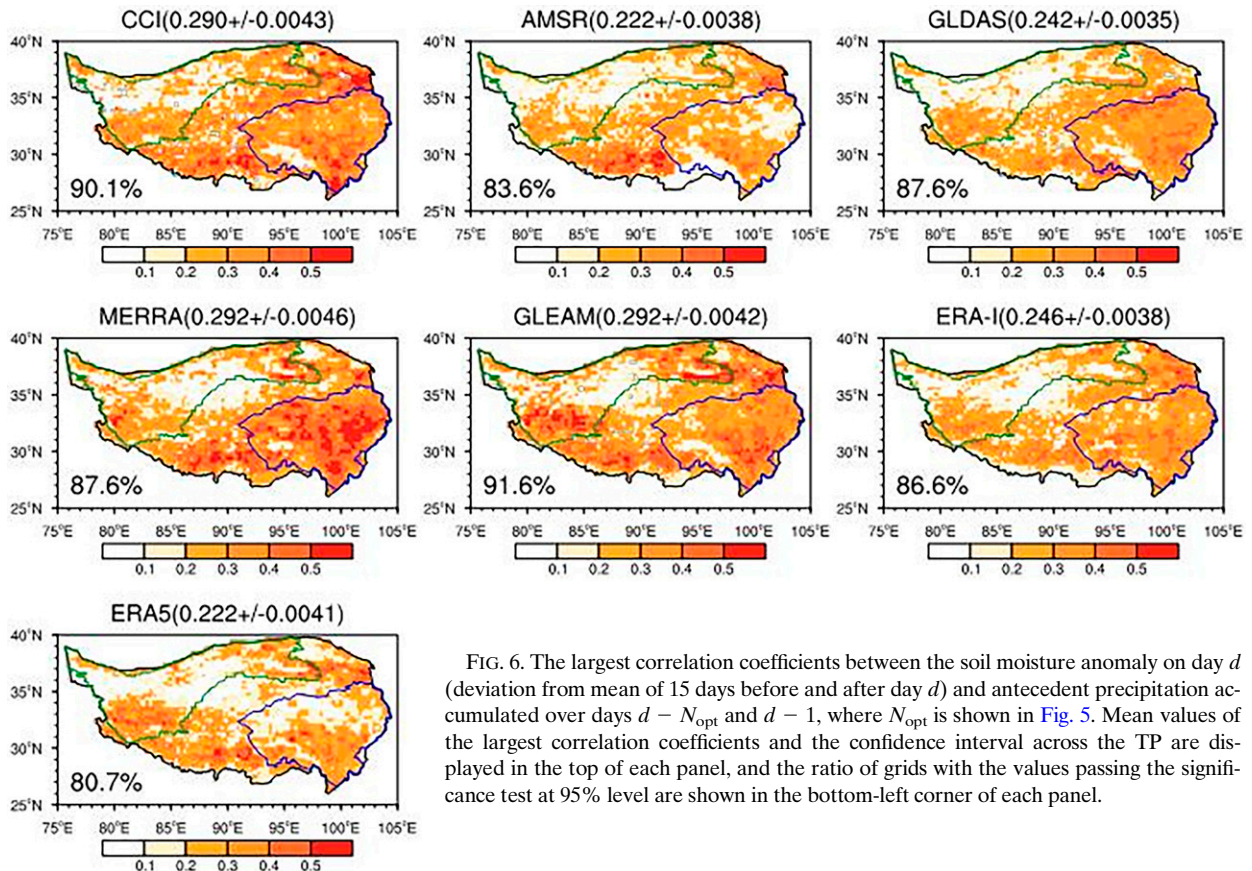


FIG. 6. The largest correlation coefficients between the soil moisture anomaly on day d (deviation from mean of 15 days before and after day d) and antecedent precipitation accumulated over days $d - N_{\text{opt}}$ and $d - 1$, where N_{opt} is shown in Fig. 5. Mean values of the largest correlation coefficients and the confidence interval across the TP are displayed in the top of each panel, and the ratio of grids with the values passing the significance test at 95% level are shown in the bottom-left corner of each panel.

soil moisture across the northwest. In terms of mean correlations across the TP, CCI, MERRA, and GLEAM perform best, with values of 0.290, 0.292, and 0.292, respectively. Considering the areal fraction with significant correlations, GLEAM and CCI score highest, 91.6% and 90.1%, respectively, illustrating a reliable relationship between soil moisture anomalies with accumulated precipitation at the weekly time scale. On the other hand, MERRA exhibits the largest correlations at the subplateau scale, with many pixels in the southeast exceeding a value of 0.5. GLDAS, ERA-I, ERA5, and AMSR products score worse in terms of TP-mean correlation coefficients. In particular, AMSR and ERA5, have correlation coefficients of 0.222 and their ratio of grids passing the significance test are lower than 85%. We also performed the same analysis with daily precipitation totals instead of accumulated precipitation values. Unsurprisingly, among all products except for MERRA, anomalous surface soil moisture is most correlated with precipitation totals at a 1- or 2-day lag (not shown). Similar to correlations with accumulated precipitation, products which include soil moisture observations, including CCI and GLEAM, have relatively high average correlation values (0.23–0.28), while those using reanalysis precipitation totals have low average correlation values (0.12–0.21; not shown). Although comparisons of instantaneous soil moisture with in situ measurements give some confidence in soil moisture products (Chen et al. 2013;

Su et al. 2013; Al-Yaari et al. 2014; Zeng et al. 2015; Zhang et al. 2018), product variability in the soil moisture response to precipitation remains a key uncertainty.

c. Soil moisture response to decadal precipitation trends

Alongside investigating differences among products in the soil moisture response to weekly precipitation variations, we have also explored how decadal soil moisture trends vary. Figure 7 shows decadal trends in boreal summer mean soil moisture, precipitation, and near-surface air temperature from 1980 to 2016. Focusing first on precipitation and air temperature trends, Fig. 7 shows significant increasing precipitation trends in parts of the west, northeast, and southeast TP. Meanwhile, a decreasing trend is observed on the eastern edge of the TP. Significant warming in the central and northern TP is also observed, with a peak warming of 0.8°C per decade.

Decadal trends in surface soil moisture vary between products with no product showing a significant trend in soil moisture anywhere on the TP. Comparing precipitation and soil moisture trends, GLEAM and ERA5 show a consistent pattern with increases across the west and central TP, and a slight reduction along the eastern edge of the TP. Discrepancies occur across the northwest of the TP, where precipitation shows an increasing trend, with GLEAM showing a positive soil moisture trend while ERA5 shows a broadly drying trend. For CCI, a purely remote sensing product, changes in the west

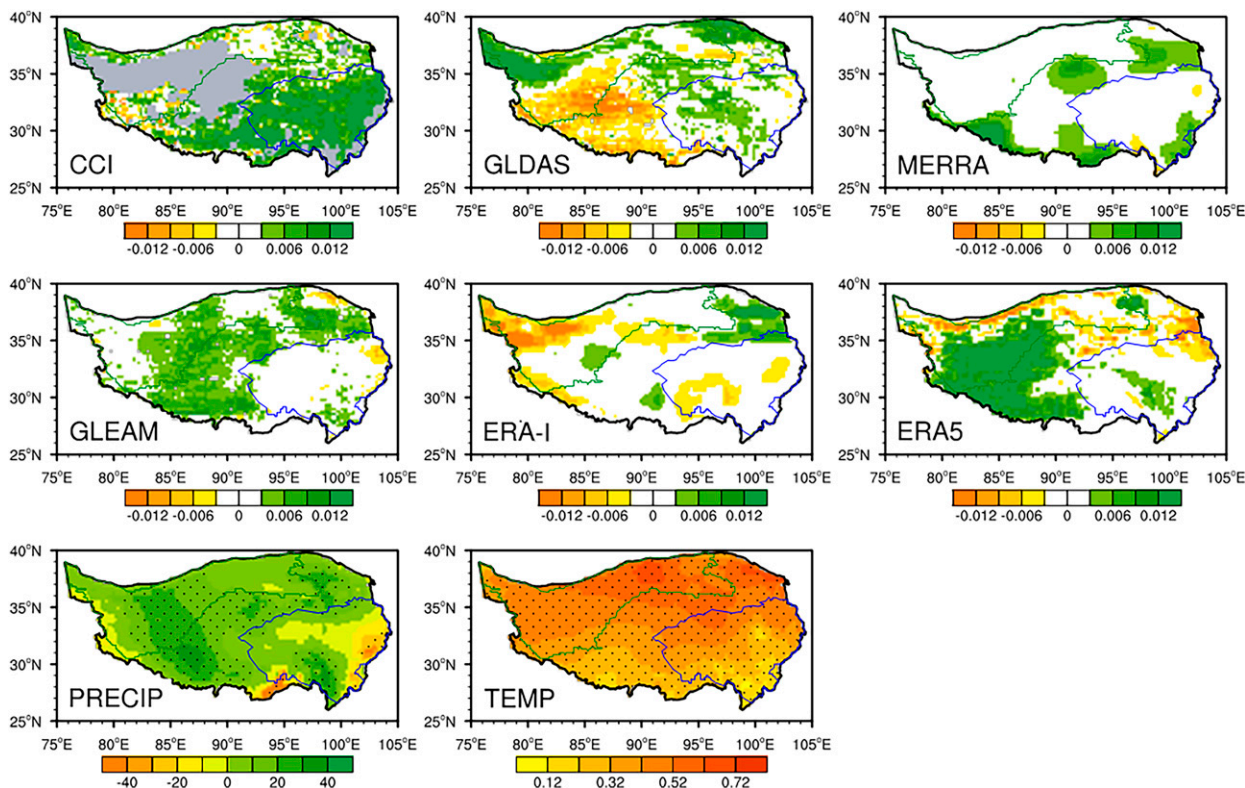


FIG. 7. Trend of soil moisture [$\text{m}^3 \text{m}^{-3} (10 \text{ yr})^{-1}$] in boreal summer for different products, air temperature [$^{\circ}\text{C} (10 \text{ yr})^{-1}$] and precipitation [$\text{mm}^{-1} (10 \text{ yr})^{-1}$ per JJA] from 1980 to 2016. The gray color masks areas with one-third of the data missing. The dots indicate the trend values that are significantly at or above 95% confidence level.

TP cannot be quantified due to missing data, while positive trends are observed across the eastern TP. In comparison to the precipitation trends, ERA-I and GLDAS exhibit quite different soil moisture trend patterns, and in places the trends are of the opposite sign to that of precipitation. For MERRA, although it is a land product with a more realistic precipitation forcing than an atmospheric reanalysis such as ERA-I and ERA5, soil moisture trends are also inconsistent with precipitation changes.

To quantify how TP soil moisture responds to different factors at the decadal scale, we compute a second-order partial correlation between JJA-average soil moisture with precipitation (Fig. 8) and surface air temperature (Fig. 9) from 1980 to 2016. Figure 8 indicates a major influence of precipitation on interannual and decadal soil moisture variability. Partial correlations of CCI and GLDAS soil moisture with precipitation show similar patterns, but with higher correlations in GLDAS. Similarly, the patterns in MERRA and GLEAM are comparable with each other and indicate significant precipitation control on soil moisture in almost all pixels outside of the northwest. The two ECMWF products show clear distinction from other products. In most regions, ERA5 soil moisture also exhibits a strong response to precipitation, but stands in contrast to the limited positive correlations in ERA-I. Considering partial correlations of soil moisture with temperature (Fig. 9), there is some interproduct consistency in the northwest edge of the TP, where there is a large area of glaciers distributed. Here, and to some extent in the south of the semiarid region, soil moisture has

a significant negative correlation with surface air temperature in ERA5, which is quite different to other products. It is noted that for ERA-I, although precipitation dominates soil moisture changes in only a limited area, surface air temperature does not show a clear influence on soil moisture either. On the other hand, in ERA5, both surface air temperature and precipitation show extensive and often strong correlations with soil moisture. We also performed the same analysis using LAI values derived from Global Land Surface Satellite (GLASS) product (Xiao et al. 2016). We observe only weak correlations between soil moisture and LAI (not shown), with some consistency across products showing a positive correlation in semiarid environments.

d. Soil moisture response to decadal precipitation across different biomes

From this analysis we can infer that across the TP changes in precipitation are primarily responsible for interannual and decadal soil moisture variability. While summer precipitation has exhibited an increase over the period 1980–2016, it is not strong enough to have driven a trend in any of these products. To explore differences in the sensitivity of soil moisture trends to precipitation due to surface biome, Fig. 10 shows a time series of boreal summer-averaged soil moisture and precipitation between 1980 and 2015 across three climate zones and the entire TP. When considering the interannual correlation between boreal summer soil moisture and precipitation, all soil moisture products show positive correlations, with values ranging from

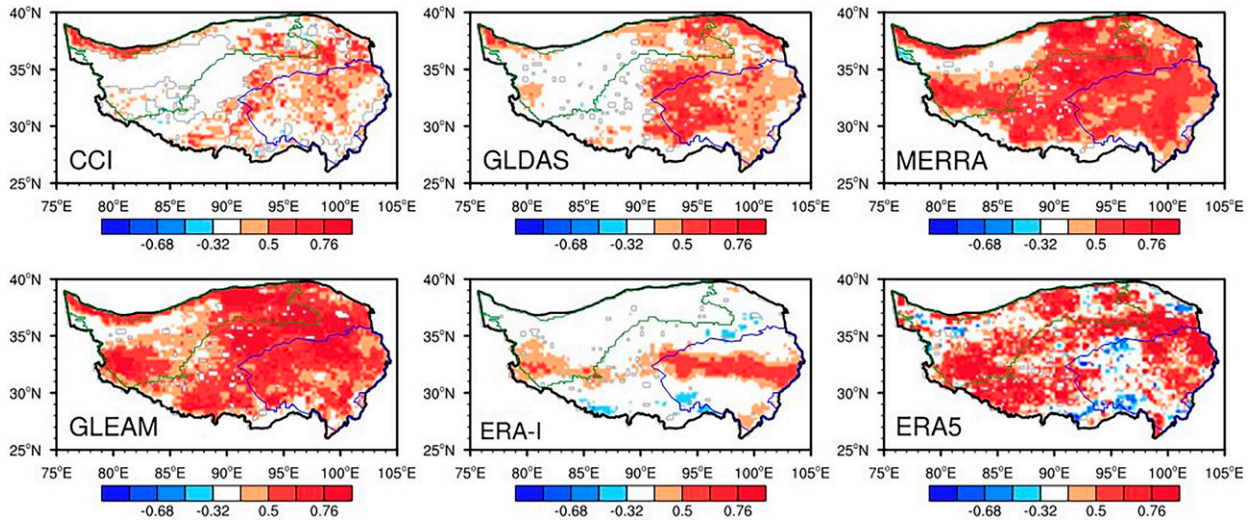


FIG. 8. Partial correlations between soil moisture and precipitation from 1980 to 2016. Correlations are only shown if significant at the 95% confidence level.

0.36 to 0.73. Correlations between GLEAM and precipitation illustrate there is a high correlation between soil moisture and precipitation. Most products show high correlation coefficients across subhumid and semiarid regions, and low correlation coefficients in arid areas due to relatively small soil moisture trends. But inconsistency across the products, for example, correlation coefficients for ERA-I in arid and subhumid regions are 0.13 and 0.59, in contrast with the values of 0.42 and 0.02 for ERA5 is presented.

4. Discussion

a. Uncertainties and ranking of the products

At weekly time scales we observe a strong soil moisture response to precipitation across all products. Pixel-wise temporal correlations between weekly accumulated antecedent

precipitation and weekly mean soil moisture anomalies substantial product variability in the soil moisture response to precipitation variability. TP-average correlation values range from 0.22 to 0.29 between different products (Table 4). The uncertainty between products is smaller in the east of the TP compared to the west, due to a higher density of rainfall gauges. This highlights the need for an increased number of in situ observational sites in the west of TP.

At interannual and decadal time scales, precipitation dominates changes in soil moisture on the TP, while air temperature and, to an even lesser extent, vegetation variability play a weaker role. Atmospheric reanalyses, including ERA-I and ERA5, are somewhat distinct from other products, with larger precipitation totals (Fig. 4) and smaller air temperatures (not shown). Decadal trends in soil moisture are insignificant across

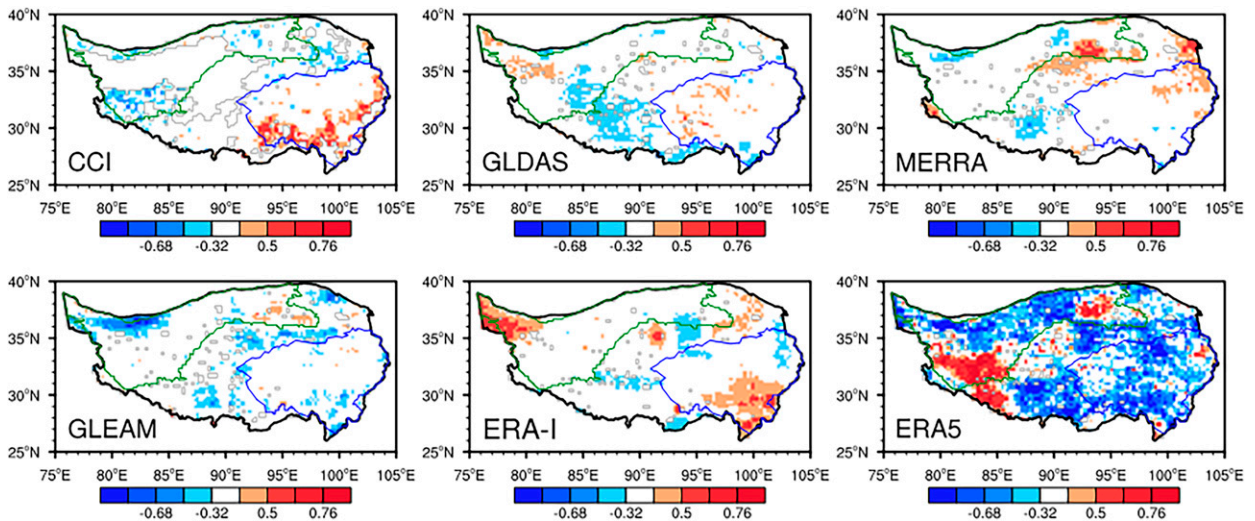


FIG. 9. Partial correlations between soil moisture and surface air temperature from 1980 to 2016. Correlations are only shown if significant at the 95% confidence level.

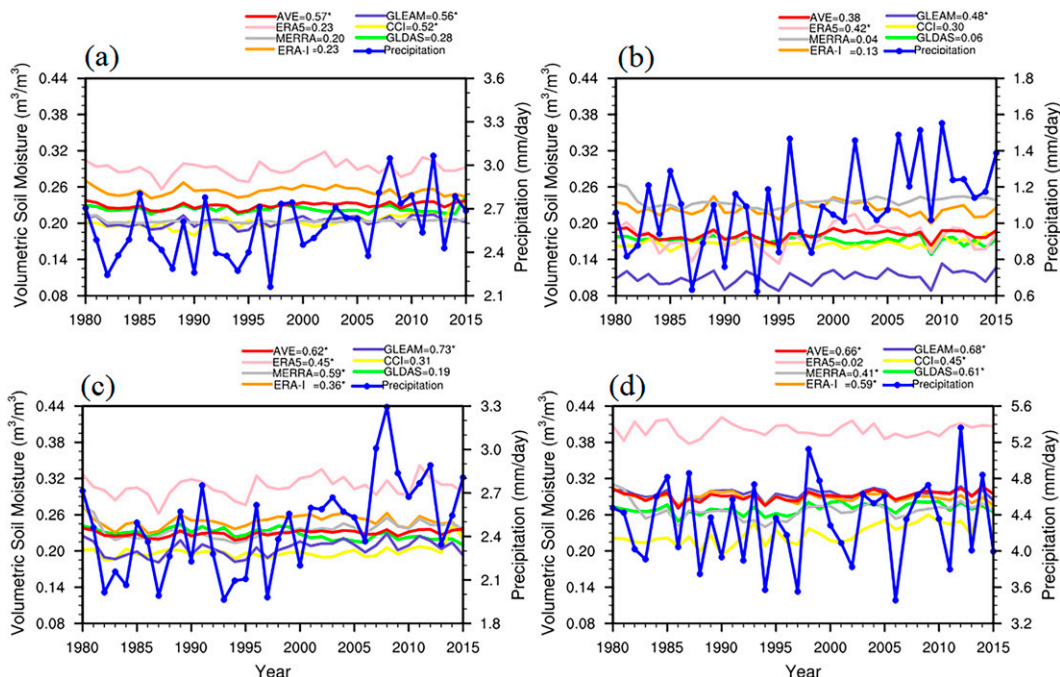


FIG. 10. Time series of JJA-average soil moisture ($\text{m}^3 \text{m}^{-3}$) and precipitation (mm day^{-1}) in the (a) TP, (b) arid area of TP, (c) semiarid area of TP, and (d) semihumid area of TP. Correlation coefficients between soil moisture and precipitation are shown above each panel, with stars showing a statistical significance at or above the 95% level. AVE denotes the average based on all soil moisture products.

different climatic zones in all products. Concerning inconsistencies among products is observed. For example, in the west of TP, GLDAS shows a decreasing decadal trend in soil moisture while GLEAM highlights an increased trend (Fig. 7).

Studies evaluating instantaneous soil moisture values with in situ observations conclude that CCI, ASCAT, and GLDAS perform well (Zeng et al. 2015; Zhang et al. 2018). In this

TABLE 4. The statistical values of soil moisture’s response to precipitation at different time scales summarized from Figs. 6 and 10. The R_{w_TP} is the mean value of the largest correlation coefficients between weekly anomalous soil moisture and accumulated precipitation on the TP (i.e., the values at top of each panel in Fig. 6), C is the ratio of grids with the values passing the significance test at 95% level in Fig. 6, R_{d_TP} is the correlation coefficient between soil moisture and precipitation in decadal time scale over the TP in Fig. 10, and R_{d_a} , R_{d_sa} , and R_{d_sh} are the same as R_{d_TP} , but for arid, semiarid, and subhumid areas, respectively.

	Weekly		Decadal			
	R_{w_TP}	C	R_{d_TP}	R_{d_a}	R_{d_sa}	R_{d_sh}
CCI	0.29	90.1	0.52	0.30	0.31	0.45
AMSR	0.22	83.6	—	—	—	—
GLDAS	0.24	87.6	0.28	0.06	0.19	0.61
GLEAM	0.29	87.6	0.56	0.48	0.73	0.68
MERRA	0.29	91.6	0.20	0.04	0.59	0.41
ERA-I	0.25	86.6	0.23	0.13	0.36	0.59
ERA5	0.22	80.7	0.23	0.42	0.45	0.02

study, we quantify the soil moisture response to precipitation at different time scales and products. Table 4 provides a summary of our analysis. We conclude that CCI is the most reliable product with robust and relatively high correlations between precipitation and soil moisture on weekly and inter-annual time scales. Land data assimilation products such as GLEAM, which are forced by observational estimates of precipitation and assimilated satellite derived soil moisture, are the next reliable soil moisture products to use. As there is no previous comparison for GLEAM with in situ observations, we calculated the correlation coefficient (R), root-mean-square error (RMSE), and mean bias as was performed in previous studies (Zeng et al. 2015; Zhang et al. 2018). Ten-centimeter-depth soil moisture observations from Maqu and Naqu soil moisture networks (Su et al. 2011; Yang et al. 2013) are used for validation (data in August 2009 and June and July 2010 for Maqu; data in August 2010 and June and July 2011 for Naqu). We conclude values of 0.66, 0.0465, and $-0.044 \text{ m}^3 \text{ m}^{-3}$, respectively, which score slightly better than CCI (0.62, 0.11, and $-0.06 \text{ m}^3 \text{ m}^{-3}$, Zeng et al. 2015). This again illustrates robust performances of CCI and GLEAM products. It is also noted that GLDAS shows a very high score when comparing instantaneous observations (Zeng et al. 2015; Zhang et al. 2018), but only shows a relatively moderate correlation in the weekly soil moisture response to accumulated precipitation (Table 4). GLDAS shows an opposite trend to decadal precipitation variations in the west of the TP compared to other products. Different skills at predicting the soil moisture response to precipitation

across different time scales could be induced by the high-quality assimilation of soil moisture in recent years. The assimilation of soil moisture may not improve predictions of decadal soil moisture changes. CCI does a poor job at decadal trend due to missing data in the west of the TP. Atmospheric reanalyses on the other hand, have a poor agreement with in situ observations (Zeng et al. 2015; Zhang et al. 2018) and a minimal soil moisture response to weekly and interannual precipitation variability. This highlights that care must be taken when using soil moisture values from reanalysis products. The best products are those which rely on surface observations, i.e., ESA CCI, or describe the physical relationship between precipitation and soil moisture well, i.e., GLEAM.

While identifying the reasons why different products exhibit a broad range of soil moisture behaviors is beyond the scope of this work, we note that products which use observational precipitation estimates, including GLEAM and MERRA, better predict the soil moisture response to precipitation. For example, GLEAM assimilates AMSR data, and as a result, outperforms the original AMSR soil moisture product. On the other hand, GLDAS scores relatively poorly in spite of observed precipitation forcing, while CCI performs well without using any meteorological data. However, there is a large fraction of missing data across the TP in the CCI product (Fig. 2). The uncertainties of the soil moisture products were found across other areas, such as in Australia, where all products in the study can better capture the interannual and seasonal variations against the in situ reference than short-term dynamics (Holgate et al. 2016). Focuses on detecting irrigation induced soil moisture variations based on different products found the uncertainties among the satellite soil moisture products in China and the northeast of the Iberian Peninsula, and they emphasized the informed assessment for purpose by the users (Escorihuela and Quintana-Seguí 2016; Qiu et al. 2016).

Due to the large area of permafrost on the TP, soil thawing could affect the soil moisture response to precipitation. For example, positive soil moisture anomalies along the northwestern edge of the TP during the second and third weeks of June can be seen in both satellite and reanalysis products (Figs. 2 and 3). For GLDAS, MERRA, and satellite-based products, we conclude that positive soil moisture anomalies are associated with increased glacial melting as soil temperatures from GLDAS and MERRA are greater than 0°C (not shown) and regions of positive anomalous soil moisture corresponds to areas where the land surface is typically categorized as seasonally frozen soil (Zou et al. 2017). But for ERA-I and ERA5, a zonal precipitation band across the northwest of the TP is the most likely cause of positive anomalous soil moisture (Fig. 4).

b. Future perspective

Alongside short-term (<3 days) precipitation-driven perturbations in soil moisture, a recent study illustrated that anomalous soil moisture on the TP can persist beyond the seasonal scale due to soil freezing (Yang and Wang 2019). In addition, land surface modeling of a site in northeast China indicated that anomalous soil moisture can persist beyond a

year, dependent on the initial soil moisture state and atmosphere condition (Song et al. 2019). Both of these studies depend on one soil moisture product or a single land surface model. Through focusing on the soil moisture response to precipitation variability on weekly time scales, we demonstrate the necessity of using multiple products to investigate soil moisture memory on the TP.

As a key parameter in land–atmosphere feedbacks, surface soil moisture can substantially affect the partitioning of the surface energy balance, local precipitation rates, and regional atmospheric circulations (Seneviratne et al. 2010). Two recent studies have highlighted that soil moisture heterogeneity plays important role on the initiation of deep convection on the TP, especially in regions with minimal vegetation and low topographic complexity (Barton et al. 2021; Zhao et al. 2022). Zhao et al. (2022) argues that surface soil moisture is a strong driver of atmospheric variability across the TP due to low near-surface air density associated with high elevation. Studies have also shown that anomalous surface soil moisture across the TP can influence local and regional atmospheric conditions and improve subseasonal predictions across much of China (Wan et al. 2017; Talib et al. 2021). In addition, Bao et al. (2010) concluded that the assimilation of satellite derived soil moisture on the TP improves the prediction of the southeast Asian monsoon onset, while Xu et al. (2013), showed that a weakening of the East Asian summer monsoon is closely associated with surface cooling on the TP. In this study we have highlighted that the soil moisture response to precipitation varies between products, therefore diagnosing the control of soil moisture on local and regional atmospheric conditions depends on the chosen soil moisture product. Future research investigating soil moisture–atmosphere feedbacks across the TP need to evaluate multiple soil moisture products.

In our analysis we focus on the shallow-layer soil moisture response to weekly precipitation accumulations and interannual variability; however, future work should investigate whether differing soil moisture responses are observed to different precipitation characteristics including precipitation intensity, frequency, and total. The combined uncertainty of the soil moisture and infiltration response to precipitation, alongside a poor understanding of thawing and glacial melt, makes it challenging to predict hydrological and atmospheric processes on the TP. Due to the arduous environment across most of the TP, most rainfall gauges and soil moisture networks are installed in low-altitude regions across the eastern TP. This study emphasizes the importance of improving instantaneous, in situ observations of both soil moisture and precipitation across other parts of the TP. An observational network across a broader area of the TP will improve our understanding of surface processes, support model development, improve the reliability of soil moisture estimates, and enhance our understanding of land–atmosphere interactions.

5. Conclusions

We investigate the soil moisture response across the TP to precipitation variability in boreal summer on weekly to decadal time scales in different products. The soil moisture

response to differences in weekly accumulated precipitation varies among products, although several products illustrate good consistency with in situ measurements. Decadal trends of boreal summer soil moisture are small across all products; meanwhile precipitation dominates interannual and decadal soil moisture variability. Through investigating the soil moisture response to precipitation variability on weekly to decadal time scales, it is clear the soil moisture response to precipitation varies between products. The results emphasize the importance of evaluating soil moisture products and setting up observations across central and west TP.

Acknowledgments. This study was conducted under the auspices of the Chinese National Science Foundation Programs (41930759, 91437102, 41822501, 41875016); Chinese Academy of Sciences (CAS) “Light of West China” Program (E2290302); The Science and Technology Research Plan of Gansu Province (20JR10RA070). JT, CT, and PW were supported by the U.K.–China Research and Innovation Partnership Fund through the Met Office Climate Science for Service Partnership (CSSP) China as part of the Newton Fund.

Data availability statement. The GLDAS data were archived at the website of the Goddard Earth Sciences Data and Information Services Center <https://disc.sci.gsfc.nasa.gov/datasets?keywords=GLDAS&page=1>. The MERRA soil moisture data were accessed at <https://disc.sci.gsfc.nasa.gov/datasets?keywords=MERRA&page=1>. The GLEAM data were accessed at <https://www.gleam.eu/>. The AMSR soil moisture data were accessed at <https://disc.sci.gsfc.nasa.gov/datasets?keywords=AMSR&page=1>. The ESA CCI soil moisture satellite data were archived at <https://www.esa-soilmoisture-cci.org/>. The ERA5 and ERA-Interim data were accessed at <https://cds.climate.copernicus.eu/cdsapp/home> and <https://apps.ecmwf.int/datasets/data/interim-full-daily/>. Observations of air temperature and precipitation at a spatial resolution of 0.5° from 1961 to 2016 and hourly precipitation product at 0.1° resolution were obtained from the National Meteorological Information Center, China Meteorological Administration (<http://data.cma.cn/site/index.html>). Observations of soil moisture at Maqu and Naqu networks are provided by Institute of Tibetan Plateau Research, Chinese Academy of Science (<http://www.tpdatabase.cn/portal/index.jsp>). GLASS LAI product was provided by Beijing Normal University Center for Global Change Data Processing and Analysis (<http://www.bnu-datacenter.com/>).

REFERENCES

- Adler, R. F., and Coauthors, 2003: The version-2 Global Precipitation Climatology Project (GPCP) monthly precipitation analysis (1979–present). *J. Hydrometeorol.*, **4**, 1147–1167, [https://doi.org/10.1175/1525-7541\(2003\)004<1147:TVGPCP>2.0.CO;2](https://doi.org/10.1175/1525-7541(2003)004<1147:TVGPCP>2.0.CO;2).
- Al-Yaari, A., and Coauthors, 2014: Global-scale comparison of passive (SMOS) and active (ASCAT) satellite based microwave soil moisture retrievals with soil moisture simulations (MERRA-land). *Remote Sens. Environ.*, **152**, 614–626, <https://doi.org/10.1016/j.rse.2014.07.013>.
- Baatz, R., and Coauthors, 2021: Reanalysis in Earth system science: Toward terrestrial ecosystem reanalysis. *Rev. Geophys.*, **59**, e2020RG000715, <https://doi.org/10.1029/2020RG000715>.
- Bao, Q., Y. Liu, J. Shi, and G. Wu, 2010: Comparisons of soil moisture datasets over the Tibetan Plateau and application to the simulation of Asia summer monsoon onset. *Adv. Atmos. Sci.*, **27**, 303–314, <https://doi.org/10.1007/s00376-009-8132-5>.
- Barton, E. J., C. M. Taylor, C. Klein, P. P. Harris, and X. Meng, 2021: Observed soil moisture impact on strong convection over mountainous Tibetan Plateau. *J. Hydrometeorol.*, **22**, 561–572, <https://doi.org/10.1175/JHM-D-20-0129.1>.
- Chen, Y., K. Yang, J. Qin, L. Zhao, W. Tang, and M. Han, 2013: Evaluation of AMSR-E retrievals and GLDAS simulations against observations of a soil moisture network on the central Tibetan Plateau. *J. Geophys. Res. Atmos.*, **118**, 4466–4475, <https://doi.org/10.1002/jgrd.50301>.
- Dai, L., and Coauthors, 2019: Seasonal dynamics and controls of deep soil water infiltration in the seasonally-frozen region of the Qinghai-Tibet plateau. *J. Hydrol.*, **571**, 740–748, <https://doi.org/10.1016/j.jhydrol.2019.02.021>.
- , R. Fu, X. Guo, Y. Du, F. Zhang, and G. Cao, 2022: Soil moisture variations in response to precipitation across different vegetation types on the northeastern Qinghai-Tibet Plateau. *Front. Plant Sci.*, **13**, 854152, <https://doi.org/10.3389/fpls.2022.854152>.
- Daly, E., and A. Porporato, 2005: A review of soil moisture dynamics: From rainfall infiltration to ecosystem response. *Environ. Eng. Sci.*, **22**, 9–24, <https://doi.org/10.1089/ees.2005.22.9>.
- Dee, D. P., and Coauthors, 2011: The ERA-Interim reanalysis: Configuration and performance of the data assimilation system. *Quart. J. Roy. Meteor. Soc.*, **137**, 553–597, <https://doi.org/10.1002/qj.828>.
- Deng, M., and Coauthors, 2020: Responses of soil moisture to regional climate change over the three rivers source region on the Tibetan Plateau. *Int. J. Climatol.*, **40**, 2403–2417, <https://doi.org/10.1002/joc.6341>.
- Derber, J. C., D. F. Parrish, and S. J. Lord, 1991: The new global operational analysis system at the National Meteorological Center. *Wea. Forecasting*, **6**, 538–547, [https://doi.org/10.1175/1520-0434\(1991\)006<0538:TNGOAS>2.0.CO;2](https://doi.org/10.1175/1520-0434(1991)006<0538:TNGOAS>2.0.CO;2).
- Duan, A., G. Wu, Y. Liu, Y. Ma, and P. Zhao, 2012: Weather and climate effects of the Tibetan Plateau. *Adv. Atmos. Sci.*, **29**, 978–992, <https://doi.org/10.1007/s00376-012-1220-y>.
- Escorihuela, M. J., and P. Quintana-Seguí, 2016: Comparison of remote sensing and simulated soil moisture datasets in Mediterranean landscapes. *Remote Sens. Environ.*, **180**, 99–114, <https://doi.org/10.1016/j.rse.2016.02.046>.
- Heisler-White, J. L., A. K. Knapp, and E. F. Kelly, 2008: Increasing precipitation event size increases aboveground net primary productivity in a semi-arid grassland. *Oecologia*, **158**, 129–140, <https://doi.org/10.1007/s00442-008-1116-9>.
- Hersbach, H., and Coauthors, 2020: The ERA5 global reanalysis. *Quart. J. Roy. Meteor. Soc.*, **146**, 1999–2049, <https://doi.org/10.1002/qj.3803>.
- Holgate, C. M., and Coauthors, 2016: Comparison of remotely sensed and modelled soil moisture data sets across Australia. *Remote Sens. Environ.*, **186**, 479–500, <https://doi.org/10.1016/j.rse.2016.09.015>.
- Holmes, T. R. H., R. A. M. De Jeu, M. Owe, and A. J. Dolman, 2009: Land surface temperature from Ka band (37 GHz)

- passive microwave observations. *J. Geophys. Res.*, **114**, D04113, <https://doi.org/10.1029/2008JD010257>.
- Immerzeel, W. W., and Coauthors, 2020: Importance and vulnerability of the world's water towers. *Nature*, **577**, 364–369, <https://doi.org/10.1038/s41586-019-1822-y>.
- Koike, T., Y. Nakamura, I. Kaihotsu, G. Davaa, N. Matsuura, K. Tamagawa, and H. Fujii, 2004: Development of an advanced microwave scanning radiometer (AMSR-E) algorithm of soil moisture and vegetation water content. *Annu. J. Hydraul. Eng.*, **48**, 217–222, <https://doi.org/10.2208/prohe.48.217>.
- Koster, R. D., and M. J. Suarez, 2001: Soil moisture memory in climate models. *J. Hydrometeorol.*, **2**, 558–570, [https://doi.org/10.1175/1525-7541\(2001\)002<0558:SMMICM>2.0.CO;2](https://doi.org/10.1175/1525-7541(2001)002<0558:SMMICM>2.0.CO;2).
- Liu, Y. Y., W. A. Dorigo, R. M. Parinussa, R. A. M. de Jeu, W. Wagner, M. F. McCabe, J. P. Evans, and A. I. J. M. van Dijk, 2012: Trend-preserving blending of passive and active microwave soil moisture retrievals. *Remote Sens. Environ.*, **123**, 280–297, <https://doi.org/10.1016/j.rse.2012.03.014>.
- Ma, N., and Y. Zhang, 2022: Increasing Tibetan Plateau terrestrial evapotranspiration primarily driven by precipitation. *Agric. For. Meteorol.*, **317**, 108887, <https://doi.org/10.1016/j.agrformet.2022.108887>.
- Ma, Y., and Coauthors, 2009: Recent advances on the study of atmosphere-land interaction observations on the Tibetan Plateau. *Hydrol. Earth Syst. Sci.*, **13**, 1103–1111, <https://doi.org/10.5194/hess-13-1103-2009>.
- Martens, B., and Coauthors, 2017: GLEAM v3: Satellite-based land evaporation and root-zone soil moisture. *Geosci. Model Dev.*, **10**, 1903–1925, <https://doi.org/10.5194/gmd-10-1903-2017>.
- Meesters, A. G. C. A., R. A. M. De Jeu, and M. Owe, 2005: Analytical derivation of the vegetation optical depth from the microwave polarization difference index. *IEEE Geosci. Remote Sens. Lett.*, **2**, 121–123, <https://doi.org/10.1109/LGRS.2005.843983>.
- Meng, X., and Coauthors, 2018: Detecting hydrological consistency between soil moisture and precipitation and changes of soil moisture in summer over the Tibetan Plateau. *Climate Dyn.*, **51**, 4157–4168, <https://doi.org/10.1007/s00382-017-3646-5>.
- Miralles, D. G., T. R. H. Holmes, R. A. M. De Jeu, J. H. Gash, A. G. C. A. Meesters, and A. J. Dolman, 2011: Global land-surface evaporation estimated from satellite-based observations. *Hydrol. Earth Syst. Sci.*, **15**, 453–469, <https://doi.org/10.5194/hess-15-453-2011>.
- Njoku, E. G., and D. Entekhabi, 1996: Passive microwave remote sensing of soil moisture. *J. Hydrol.*, **184**, 101–129, [https://doi.org/10.1016/0022-1694\(95\)02970-2](https://doi.org/10.1016/0022-1694(95)02970-2).
- , and S. K. Chan, 2006: Vegetation and surface roughness effects on AMSR-E land observations. *Remote Sens. Environ.*, **100**, 190–199, <https://doi.org/10.1016/j.rse.2005.10.017>.
- , T. J. Jackson, V. Lakshmi, T. K. Chan, and S. V. Nghiem, 2003: Soil moisture retrieval from AMSR-E. *IEEE Trans. Geosci. Remote Sens.*, **41**, 215–229, <https://doi.org/10.1109/TGRS.2002.808243>.
- , P. Ashcroft, T. K. Chan, and L. Li, 2005: Global survey and statistics of radio-frequency interference in AMSR-E land observations. *IEEE Trans. Geosci. Remote Sens.*, **43**, 938–947, <https://doi.org/10.1109/TGRS.2004.837507>.
- Oliver, J. E., 1980: Monthly precipitation distribution: A comparative index. *Prof. Geogr.*, **32**, 300–309, <https://doi.org/10.1111/j.0033-0124.1980.00300.x>.
- Owe, M., R. de Jeu, and J. Walker, 2001: A methodology for surface soil moisture and vegetation optical depth retrieval using the microwave polarization difference index. *IEEE Trans. Geosci. Remote Sens.*, **39**, 1643–1654, <https://doi.org/10.1109/36.942542>.
- , —, and T. Holmes, 2008: Multisensor historical climatology of satellite-derived global land surface moisture. *J. Geophys. Res.*, **113**, F01002, <https://doi.org/10.1029/2007JF000769>.
- Qiu, J., Q. Gao, S. Wang, and Z. Su, 2016: Comparison of temporal trends from multiple soil moisture data sets and precipitation: The implication of irrigation on regional soil moisture trend? *Int. J. Appl. Earth Obs. Geoinf.*, **48**, 17–27, <https://doi.org/10.1016/j.jag.2015.11.012>.
- Rienecker, M. M., and Coauthors, 2011: MERRA: NASA's Modern-Era Retrospective Analysis for Research and Applications. *J. Climate*, **24**, 3624–3648, <https://doi.org/10.1175/JCLI-D-11-00015.1>.
- Rodell, M., and Coauthors, 2004: The Global Land Data Assimilation System. *Bull. Amer. Meteor. Soc.*, **85**, 381–394, <https://doi.org/10.1175/BAMS-85-3-381>.
- Seneviratne, S. I., T. Corti, E. L. Davin, M. Hirschi, E. B. Jaeger, I. Lehner, B. Orlowsky, and A. J. Teuling, 2010: Investigating soil moisture-climate interactions in a changing climate: A review. *Earth-Sci. Rev.*, **99**, 125–161, <https://doi.org/10.1016/j.earscirev.2010.02.004>.
- Sheffield, J., G. Goteti, and E. F. Wood, 2006: Development of a 50-year high-resolution global dataset of meteorological forcings for land surface modeling. *J. Climate*, **19**, 3088–3111, <https://doi.org/10.1175/JCLI3790.1>.
- Song, Y. M., Z. F. Wang, L. L. Qi, and A. N. Huang, 2019: Soil moisture memory and its effect on the surface water and heat fluxes on seasonal and interannual time scales. *J. Geophys. Res. Atmos.*, **124**, 10730–10741, <https://doi.org/10.1029/2019JD030893>.
- Su, Z., J. Wen, L. Dente, R. van der Velde, L. Wang, Y. Ma, K. Yang, and Z. Hu, 2011: The Tibetan Plateau observatory of plateau scale soil moisture and soil temperature (Tibet-Obs) for quantifying uncertainties in coarse resolution satellite and model products. *Hydrol. Earth Syst. Sci.*, **15**, 2303–2316, <https://doi.org/10.5194/hess-15-2303-2011>.
- , P. de Rosnay, J. Wen, L. Wang, and Y. Zeng, 2013: Evaluation of ECMWF's soil moisture analyses using observations on the Tibetan Plateau. *J. Geophys. Res. Atmos.*, **118**, 5304–5318, <https://doi.org/10.1002/jgrd.50468>.
- Sun, F., Y. Lüa, J. Wang, J. Hu, and B. Fu, 2015: Soil moisture dynamics of typical ecosystems in response to precipitation: A monitoring-based analysis of hydrological service in the Qilian Mountains. *Catena*, **129**, 63–75, <https://doi.org/10.1016/j.catena.2015.03.001>.
- Talib, J., C. M. Taylor, A. Duan, and A. G. Turner, 2021: Intra-seasonal soil moisture-atmosphere feedbacks on the Tibetan Plateau circulation. *J. Climate*, **34**, 1789–1807, <https://doi.org/10.1175/JCLI-D-20-0377.1>.
- Wagner, W., Z. Bartalis, V. Naeimi, S.-E. Park, J. Figa-Saldaña, and H. Bonekamp, 2010: Status of the METOP ASCAT soil moisture product. *30th IEEE Int. Geoscience and Remote Sensing Symp. (IGARSS) on Remote Sensing—Global Vision for Local Action*, Honolulu, HI, Institute of Electrical and Electronics Engineers, 276–279, <https://doi.org/10.1109/IGARSS.2010.5653358>.
- , W. Dorigo, R. de Jeu, D. Fernandez, J. Benveniste, E. Haas, and M. Ert, 2012: Fusion of active and passive microwave observations to create an Essential Climate Variable data record on soil moisture. *ISPRS Ann. Photogramm.*

- Remote Sens. Spatial Inf. Sci.*, **1-7**, 315–321, <https://doi.org/10.5194/isprsannals-1-7-315-2012>.
- Wan, B., Z. Gao, F. Chen, and C. Lu, 2017: Impact of Tibetan Plateau surface heating on persistent extreme precipitation events in southeastern China. *Mon. Wea. Rev.*, **145**, 3485–3505, <https://doi.org/10.1175/MWR-D-17-0061.1>.
- Wu, G., Y. Liu, B. Dong, X. Liang, A. Duan, Q. Bao, and J. Yu, 2012: Revisiting Asian monsoon formation and change associated with Tibetan Plateau forcing: I. Formation. *Climate Dyn.*, **39**, 1169–1181, <https://doi.org/10.1007/s00382-012-1334-z>.
- Xiao, Z., S. Liang, J. Wang, Y. Xiang, X. Zhao, and J. Song, 2016: Long-time-series global land surface satellite leaf area index product derived from MODIS and AVHRR surface reflectance. *IEEE Trans. Geosci. Remote Sens.*, **54**, 5301–5318, <https://doi.org/10.1109/TGRS.2016.2560522>.
- Xu, X., C. Lu, Y. Ding, X. Shi, Y. Guo, and W. Zhu, 2013: What is the relationship between China summer precipitation and the change of apparent heat source over the Tibetan Plateau? *Atmos. Sci. Lett.*, **14**, 227–234, <https://doi.org/10.1002/asl2.444>.
- Yan, D., N. Ma, and Y. Zhang, 2022: Development of a fine-resolution snow depth product based on the snow cover probability for the Tibetan Plateau: Validation and spatial-temporal analyses. *J. Hydrol.*, **604**, 127027, <https://doi.org/10.1016/j.jhydrol.2021.127027>.
- Yang, K., and C. Wang, 2019: Seasonal persistence of soil moisture anomalies related to freeze–thaw over the Tibetan Plateau and prediction signal of summer precipitation in eastern China. *Climate Dyn.*, **53**, 2411–2424, <https://doi.org/10.1007/s00382-019-04867-1>.
- , and Coauthors, 2013: A multiscale soil moisture and freeze–thaw monitoring network on the third pole. *Bull. Amer. Meteor. Soc.*, **94**, 1907–1916, <https://doi.org/10.1175/BAMS-D-12-00203.1>.
- Yao, T., and Coauthors, 2012: Different glacier status with atmospheric circulations in Tibetan Plateau and surroundings. *Nat. Climate Change*, **2**, 663–667, <https://doi.org/10.1038/nclimate1580>.
- , G. Wu, B. Xu, W. Wang, J. Gao, and B. An, 2019: Asian water tower change and its impacts (in Chinese). *Bull. Chin. Acad. Sci.*, **34**, 1203–1209, <https://doi.org/10.16418/j.issn.1000-3045.2019.11.003>.
- , and Coauthors, 2022: The imbalance of the Asian water tower. *Nat. Rev. Earth Environ.*, **3**, 618–632, <https://doi.org/10.1038/s43017-022-00299-4>.
- You, Q., J. Min, Y. Jiao, M. Sillanpaa, and S. Kang, 2016: Observed trend of diurnal temperature range in the Tibetan Plateau in recent decades. *Int. J. Climatol.*, **36**, 2633–2643, <https://doi.org/10.1002/joc.4517>.
- Zeng, J., Z. Li, Q. Chen, H. Bia, J. Qiu, and P. Zou, 2015: Evaluation of remotely sensed and reanalysis soil moisture products over the Tibetan Plateau using in-situ observations. *Remote Sens. Environ.*, **163**, 91–110, <https://doi.org/10.1016/j.rse.2015.03.008>.
- Zhang, Q., K. Fan, V. P. Singh, P. Sun, and P. Shi, 2018: Evaluation of remotely sensed and reanalysis soil moisture against in situ observations on the Himalayan-Tibetan Plateau. *J. Geophys. Res. Atmos.*, **123**, 7132–7148, <https://doi.org/10.1029/2017JD027763>.
- Zhao, C., X. Meng, Y. Li, S. Lyu, J. Guo, and H. Liu, 2022: Impact of soil moisture on afternoon convection triggering over the Tibetan Plateau based on 1-D boundary layer model. *J. Geophys. Res. Atmos.*, **127**, e2021JD035591, <https://doi.org/10.1029/2021JD035591>.
- Zhao, Y., J. Zhu, and Y. Xu, 2014: Establishment and assessment of the grid precipitation datasets in China for recent 50 years (in Chinese). *J. Meteor. Sci.*, **34**, 414–420, <https://doi.org/10.3969/2013jms.0008>.
- Zhu, X., and Coauthors, 2017: Impacts of summer extreme precipitation events on the hydrothermal dynamics of the active layer in the Tanggula permafrost region on the Qinghai-Tibetan Plateau. *J. Geophys. Res. Atmos.*, **122**, 11 549–11 567, <https://doi.org/10.1002/2017JD026736>.
- Zou, D., and Coauthors, 2017: A new map of permafrost distribution on the Tibetan Plateau. *Cryosphere*, **11**, 2527–2542, <https://doi.org/10.5194/tc-11-2527-2017>.